



HAL
open science

Absolute Age and Temperature Constraints on Deformation Along the Basal Décollement of the Jura Fold-and-Thrust Belt From Carbonate U-Pb Dating and Clumped Isotopes

N. Looser, H. Madritsch, M. Guillong, Oscar Laurent, S. Wohlwend, S. Bernasconi

► To cite this version:

N. Looser, H. Madritsch, M. Guillong, Oscar Laurent, S. Wohlwend, et al.. Absolute Age and Temperature Constraints on Deformation Along the Basal Décollement of the Jura Fold-and-Thrust Belt From Carbonate U-Pb Dating and Clumped Isotopes. *Tectonics*, 2021, 40 (3), 10.1029/2020TC006439. hal-03436604

HAL Id: hal-03436604

<https://hal.science/hal-03436604>

Submitted on 29 Nov 2021

HAL is a multi-disciplinary open access archive for the deposit and dissemination of scientific research documents, whether they are published or not. The documents may come from teaching and research institutions in France or abroad, or from public or private research centers.

L'archive ouverte pluridisciplinaire **HAL**, est destinée au dépôt et à la diffusion de documents scientifiques de niveau recherche, publiés ou non, émanant des établissements d'enseignement et de recherche français ou étrangers, des laboratoires publics ou privés.



Distributed under a Creative Commons Attribution - NoDerivatives 4.0 International License

Tectonics

RESEARCH ARTICLE

10.1029/2020TC006439

Key Points:

- Propagation of Alpine deformation along the basal décollement into the distal foreland initiated at 14.3 Ma at the latest
- Deformation occurred over a time period of at least ~10 Ma (14.3–4.5 Ma) with contemporaneous activity of thrusts and strike-slip faults
- Constant in situ temperatures and fluid sources show that large-scale foreland erosion did not initiate before 4.5 Ma

Supporting Information:

- Supporting Information S1

Correspondence to:

N. Looser,
nathan.looser@erdw.ethz.ch

Citation:

Looser, N., Madritsch, H., Guillong, M., Laurent, O., Wohlwend, S., & Bernasconi, S. M. (2021). Absolute age and temperature constraints on deformation along the basal décollement of the Jura fold-and-thrust belt from carbonate U-Pb dating and clumped isotopes. *Tectonics*, 40, e2020TC006439. <https://doi.org/10.1029/2020TC006439>

Received 23 JUL 2020

Accepted 24 DEC 2020

© Wiley Periodicals LLC. The Authors. This is an open access article under the terms of the [Creative Commons Attribution License](https://creativecommons.org/licenses/by/4.0/), which permits use, distribution and reproduction in any medium, provided the original work is properly cited.

Absolute Age and Temperature Constraints on Deformation Along the Basal Décollement of the Jura Fold-and-Thrust Belt From Carbonate U-Pb Dating and Clumped Isotopes

N. Looser¹ , H. Madritsch² , M. Guillong¹ , O. Laurent¹ , S. Wohlwend¹, and S. M. Bernasconi¹ 

¹Department of Earth Sciences, ETH Zurich, Zurich, Switzerland, ²Swiss National Cooperative for the Disposal of Radioactive Waste (Nagra), Wettingen, Switzerland

Abstract During its late-stage evolution, the European Alpine orogen witnessed a northwest-directed propagation of its deformation front along an evaporitic basal décollement into the foreland. This resulted in the decoupling of the northern Alpine Molasse Basin from its basement and the formation of the Jura fold-and-thrust belt. Here, we present the first absolute age and temperature constraints on deformation along this basal décollement using carbonate U-Pb LA-ICP-MS dating and clumped isotope thermometry. We analyzed calcite veins associated with a thrust fault branching off from the basal décollement in the distal Molasse Basin and slickenfibers from thrusts and strike-slip faults in the eastern Jura Mountains. Our U-Pb data provide evidence for tectonic activity related to Alpine contraction between 14.3 and 4.5 Ma ago. According to the oldest deformation ages, the propagation of Alpine deformation into the distal foreland along the basal décollement occurred earlier than previously inferred by biostratigraphy, at Middle Miocene (Langhian) times at the latest. Younger deformation ages between 11.3 and 4.5 Ma correspond very well in time with shortening in the Subalpine Molasse and the Central Alps, proving simultaneous tectonic activity along both thrust fronts; i.e., the Jura Mountains and the Subalpine Molasse. Clumped isotopes reveal vein calcite precipitation at temperatures between 53 and 104 °C from fluids with oxygen isotope compositions between −6.2‰ and +9.5‰ reflecting distinct burial settings. Combined, our U-Pb and clumped isotope data show that the burial conditions in the studied area remained constant between 14.3 and 4.5 Ma indicating that large-scale foreland erosion did not initiate before 4.5 Ma.

1. Introduction

The timing of formation and the deformation sequence of foreland fold-and-thrust belts provide fundamental constraints for geodynamic reconstructions of convergent orogens (Pfiffner, 2017; Poblet & Lisle, 2011). Besides the timing, the temperature conditions and fluid flow during deformation are further key parameters for understanding foreland fold-and-thrust belt evolution as the kinematics of viscous décollement-based thrust systems is known to be strongly governed by temperature and fluid circulation (e.g., Nemcok et al., 2009). The most direct way to derive these key parameters is to access syntectonic carbonate vein cements that precipitated in fractures related to the foreland thrust system during times of tectonic activity. The elemental and isotopic compositions of such cements record both the timing of mineralization (corresponding to the vein-forming tectonic event) as well as the temperature and composition of the parent fluid. Combining the information obtained from multiple generations of carbonate vein cements provides a series of snapshots reflecting temperatures and fluid compositions prevailing at specific points in time and allows to constrain the tectonic and thermal evolution of the foreland fold-and-thrust belt.

Recent progress in carbonate U-Pb laser ablation inductively coupled plasma mass spectrometry (LA-ICP-MS) has opened new perspectives in accessing carbonate cements for direct dating of complex, multiphase deformation histories (e.g., Beaudoin et al., 2018; Nuriel et al., 2017; Parrish et al., 2018). Carbonate clumped isotope thermometry, on the other hand, has proven to be a valuable tool to directly reconstruct temperatures and fluid flow during fault movement, also in low-temperature systems where other paleothermometers are scarce and without the need for assumptions as is the case for the traditional $\delta^{18}\text{O}$ paleothermometer (e.g.,

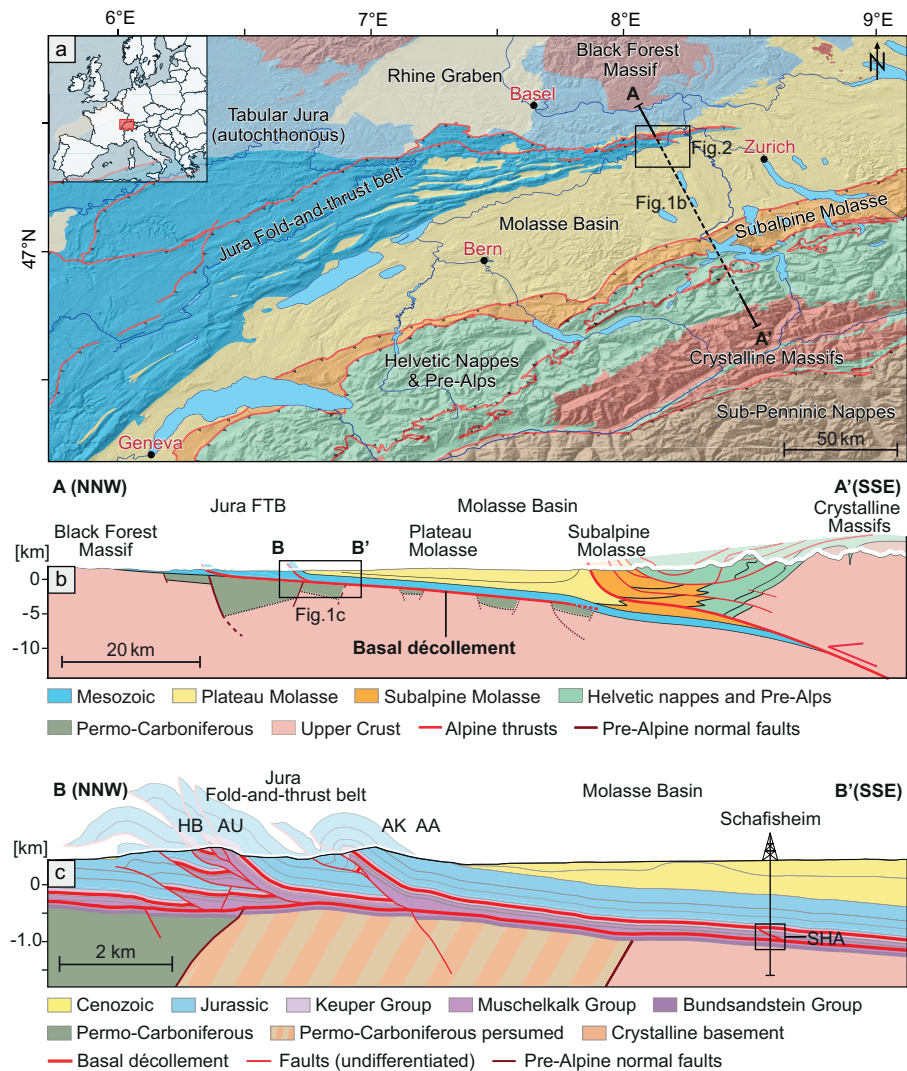


Figure 1. (a) Simplified tectonic map of the Central European Alps and their northwestern foreland. (b) Regional transect with the basal décollement of the Alpine foreland linking the Alps with the Jura fold-and-thrust belt. Figures 1a and 1b modified after Pfiffner (2014). (c) Close-up section across the Schafisheim (SHA) borehole in the distal northern part of the Molasse Basin just south of the Jura range (HB, Habsburg; AU, Asp-Ueslimatt; AK, Asperchus; AA, Aaretal-Auenstein). Abbreviations indicate the approximate locations of the studied faults. Figure 1c modified after Jordan et al. (2015).

Bergman et al., 2013; Fernandez et al., 2017; Huntington & Lechler, 2015; Smeraglia et al., 2020). Coupled as $\Delta_{47}/(U\text{-Pb})$ thermochronometer (e.g., Manganot et al., 2018), the two methods are a strong tool allowing to obtain fundamental new insights into the geodynamic evolution of foreland fold-and-thrust belts. In this study, we apply carbonate U-Pb LA-ICP-MS dating and clumped isotope thermometry on vein calcites to constrain deformation along the basal décollement of the Jura Mountains, a classic example of a thin-skinned fold-and-thrust belt in the northwestern foreland of the European Alps.

The Jura Mountains, where the basal décollement crops out at the surface, form the most external part of the northwestern Alpine foreland thrust system (Burkhard, 1990; Burkhard & Sommaruga, 1998). To the south, the Cenozoic Molasse Basin between the Jura Mountains and the Alpine front lies above the basal décollement that links the two mountain chains with each other (Figure 1). In the more distal parts of the Molasse Basin, the basin infill is only mildly deformed due to passive transport along the basal décollement (Plateau Molasse, Figure 1b). In the more proximal parts, however, the basin infill is incorporated into a triangle zone that involves a unit of thrust imbricates (Subalpine Molasse). These thrust imbricates relate to a thrust horizon on top of the Mesozoic sequence that merges with the deeper-seated basal décollement further to the south.

The formation of the Jura Mountains is coupled to the late-stage evolution of the Alpine orogen and is associated with a northwest-directed propagation of the Alpine front of up to 80 km into the foreland (Figures 1a and 1b; Burkhard, 1990; Laubscher, 1978; Pfiffner, 1986). It has been related to Miocene upper crustal nappe stacking in the Central Alps due to plate convergence (“distant push” hypothesis; Burkhard & Sommaruga, 1998; Buxtorf, 1907; Laubscher, 1978). Deformation propagated into the foreland in a thin-skinned manner along the shallow dipping thrust décollement in rheologically weak Triassic evaporites near the base of the Mesozoic succession below the Molasse Basin (Figures 1b and 1c; Philippe et al., 1996; Sommaruga et al., 2017). The basal décollement comprises two main levels that are located within the evaporitic successions of the Triassic Keuper and Muschelkalk groups. Deformation associated with the décollement occurs in both levels as well as connecting the two levels (Sommaruga et al., 2017, and references therein). During or slightly after the formation of the Jura Mountains, the Molasse Basin experienced a phase of uplift and kilometer-scale erosion. The exact timing of the onset and the amount of erosion as well as its cause (climate, crustal deformation, or deep mantle processes) is still a subject of debate (Burkhard & Sommaruga, 1998; Cederbom et al., 2004; Mazurek et al., 2006; Schlunegger & Mosar, 2011; Von Hagke et al., 2012; Willett & Schlunegger, 2010).

To date, no absolute and direct age and temperature data for thin-skinned thrusting along the basal décollement are available. Temporal constraints for the formation of the Jura Mountains are sparse and mostly based on relative age constraints from locally preserved Molasse deposits showing signs of deformation and being dated by biostratigraphy. Seismic observations in the most distal part of the foreland basin and the youngest Molasse deposits found in synclines of the Jura Mountains suggest that the main phase of folding in this area occurred after ~12 Ma (Becker, 2000, and references therein; Malz et al., 2016; Sommaruga et al., 1995). Along the northern margin of the Jura Mountains, biostratigraphic ages of Molasse deposits in synclines and over-thrusted Molasse north of the Jura frontal thrust suggest an earliest possible onset of northernmost folding and frontal thrusting at ~11 Ma (Kälin, 1997). An estimate for the latest age of folding in the Jura mountains of ~3 Ma was derived based on tectonically undisturbed (postfolding) karst infills (Bolliger et al., 1993). A similar time frame of ~9-3 Ma was suggested for frontal thrusting along the western Jura margin along the Bresse Graben (Becker, 2000, and references therein). Notably, some authors have argued for a much earlier onset of Alpine foreland thrusting in the western proximal Molasse Basin based on the interpretation of syntectonic Early Miocene (Burdigalian, ~20-16 Ma) Molasse sediments located close to the Alpine front (Beck et al., 1998; Deville et al., 1994; Pfiffner, 2014). While valuable as brackets of deformation timing, the existing relative age constraints have several limitations: (1) They only provide minimum and maximum age constraints on deformation and do not allow for differentiation between individual tectonic events. (2) It is not unequivocally sure to what extent the maximum age constraints from the distal foreland are representative for faulting along the basal décollement underneath the Molasse Basin where the foreland decoupling occurred. (3) Interpretations based on the youngest deformed Molasse deposits are hampered by the fact that these have been affected by erosion (e.g., Cederbom et al., 2004; Mazurek et al., 2006) so that maximum deformation ages based upon them are potentially overestimated (too old).

Previous estimations of the ambient temperatures during deformation along the basal décollement depend mainly on assumptions on the thickness of the Mesozoic and Cenozoic sedimentary overburden as well as on the geothermal gradient. Accordingly, temperatures during deformation along the evaporitic basal décollement are thought to generally decrease from 200 °C in the proximal parts of the Molasse basin close to the Alps to about 40 °C in the Jura Mountains (Sommaruga et al., 2017). Recently, temperatures between 10 °C and 54 °C were reconstructed for fluids associated with the Fuans thrust located in the Late Jurassic limestones of the Internal Jura of eastern France using clumped isotopes (Smeraglia et al., 2020). These temperature data, however, were obtained from samples in surface outcrops >1 km above the basal décollement and as such do not record ambient temperatures at the décollement.

Our combined clumped isotope and U-Pb data of vein calcites provide the first absolute deformation ages and reconstructions of the temperatures and fluid sources under which the deformation along the basal décollement of the northern Alpine foreland took place. Beyond that, this case-study of the Jura Mountains illustrates the potential of this conceptual and methodological approach for unraveling multiphase tectonic histories of orogenic forelands in general.

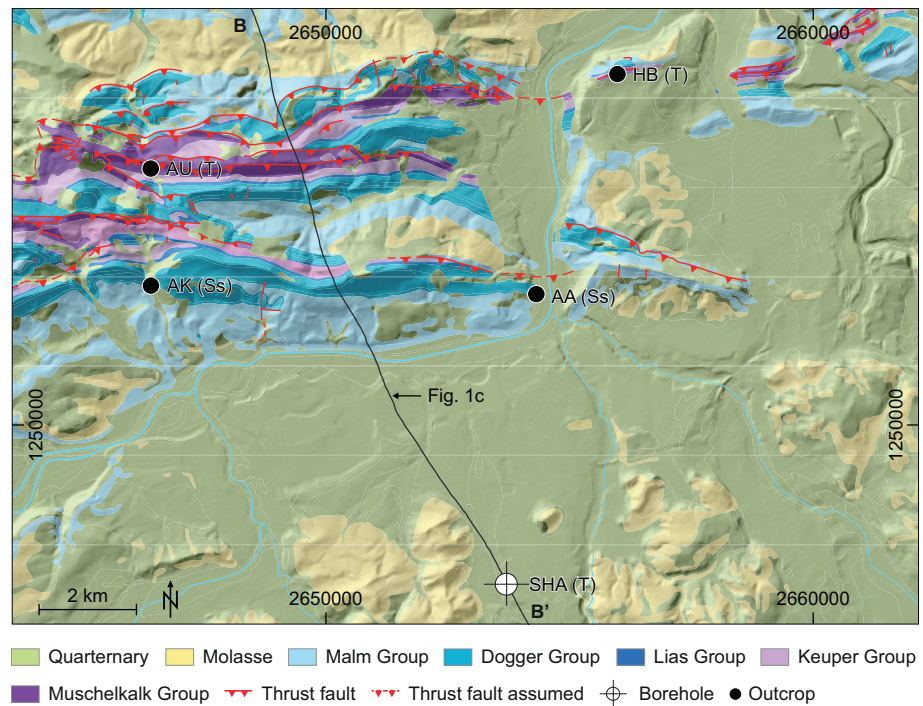


Figure 2. Detailed geological map of the study area with the locations of the sampled thrusts (marked with T: SHA, AU, HB) and strike-slip faults (marked with Ss: AA, AK). The black line indicates the close-up section of Figure 1c. Coordinates are given in Swiss Coordinates CH1903+.

2. Conceptual Approach

Vein cements within the evaporitic basal décollement are typically composed of anhydrite and are not suitable for U-Pb geochronology and clumped isotope thermometry. To overcome this, we analyzed calcite veins associated with thrust faults located between the two main levels of the basal décollement. Based on thrust orientations, kinematic indicators such as slickenfibers on fault planes, the local tectonic context, and in one case the direct connection to the lower of the two main décollement levels (see also Section 3), these thrusts all can be shown to have formed in kinematic relation to deformation along the basal décollement due to Alpine shortening. The investigated thrusts have stratigraphic positions very close to the main thrust horizon above the mechanical basement. Therefore, the sampled vein calcites reflect both timing and burial conditions during tectonic activity along the basal décollement. We investigated three thrusts that are located in two different tectonic domains; the distal Molasse Basin and the Internal Jura Mountains (Figures 1 and 2). These thrusts cannot directly be related to each other as they do not share the exact same tectonic context (see Section 3). Nevertheless, they allow to compare the timing and burial conditions during deformation along a N-S transect across the two tectonic domains. For accessing the basal décollement within the Molasse Basin, where it is buried throughout, we take advantage of the unique sampling opportunity from drill cores of a deep exploration borehole (Schafisheim well, Figures 1c and 2). In addition to the thrusts, we sampled two typical outcrop-scale strike-slip faults located in the Middle Jurassic succession of the Internal Jura Mountains. This allows for a comparison between the timing of thrusting and strike-slip faulting in the Jura fold-and-thrust belt.

3. Tectonic Context

3.1. Schafisheim Thrust

The Schafisheim borehole (WGS 84: 47.36950°N, 8.14855°E; Matter et al., 1988a, 1988b) is located ~5 km south of the Jura Mountains and ~45 km north of the topographic break related to the frontal thrust of the Subalpine Molasse (Figure 1). Drill cores were retrieved from most of the basal décollement and

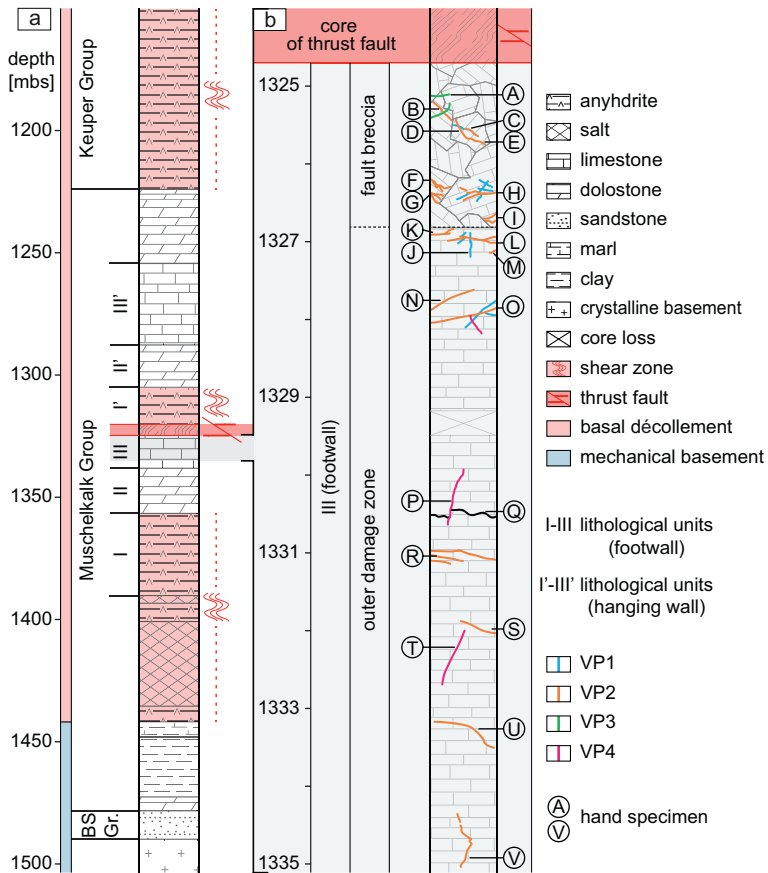


Figure 3. (a) Section through the Middle Triassic succession at Schafisheim with the SHA thrust located between the two evaporitic main levels of the basal décollement resulting in a repeated succession (lithological units I–III and I'–III' in the foot and hanging wall, respectively). (b) Close-up sketch of the SHA thrust with the sampled veins (simplified). Capital letters refer to hand specimens (A–V) containing analyzed veins (e.g., B-a and B-b; see Figure 5 and supporting information). Attributed colors indicate vein populations (VP1 veins in blue, VP2 in orange, VP3 in green, and VP4 in pink; based on crosscutting relationships and vein orientations, see Section 5.1).

structurally analyzed in detail (e.g., Jordan & Nüesch, 1989; Matter et al., 1988a, 1988b). Accordingly, the evaporites of the Triassic Keuper and Muschelkalk groups are the main constituents of the basal décollement at this location and a strongly tectonized salt and anhydrite sequence (1,393.35–1,435.43 m; Figure 3) forms the main thrust horizon above the mechanical basement. A thrust fault (herein called SHA thrust) is located between the two major evaporitic deformation levels and juxtaposes rheologically weak anhydrite-bearing dolostones and marls of the basal décollement on top of rigid limestones. This is shown by a repeated succession within the Muschelkalk Group (lithological units I–III in the footwall and I'–III' in the hanging wall; Figure 3a; simplified after Matter et al. (1988a, 1988b)) and also based on seismic reflection data indicate a splay structure of the underlying evaporitic basal décollement (Jordan et al., 2015). The core of this thrust fault (1,320.15–1,324.70 m) consists of a brecciated dolostone in a claystone-anhydrite matrix and is strongly sheared along subhorizontal fault planes. In the underlying footwall of the thrust, a ~10 m thick damage zone of deformed limestones (Figure 3b; lithological unit III at 1,324.70–1,335.26 m) is developed. The uppermost 2 m (1,324.70–1,326.81 m) of this damage zone constitute a cataclastic fault breccia with rotated limestone fragments, sometimes showing subvertically oriented sedimentary bedding planes in the otherwise subhorizontally layered sequence (Figure 3b). In the underlying outer damage zone, the sedimentary fabric is intact. A dense network of calcite veins pervades both the cataclastic fault breccia and the outer damage zone of the thrust's footwall from which samples were collected.

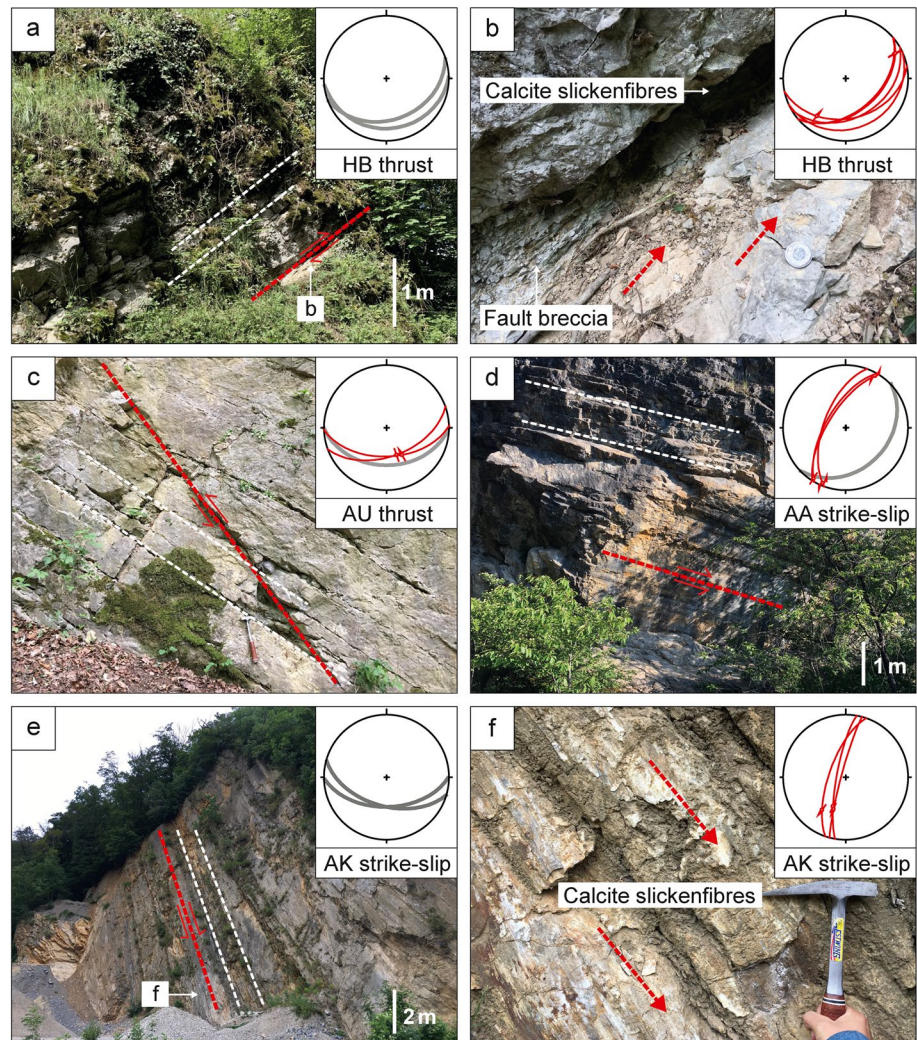


Figure 4. Field impressions of the sampled thrusts and strike-slip faults in the eastern Jura Mountains (see Figure 2 for locations). The white lines indicate the bedding orientations. The red lines indicate the sampled faults (a and c) or fault-slip lineation (b, d, e, and f). Arrows in photographs indicate slip directions parallel to the fault plane lineation. Stereo plots are lower hemisphere, equal area projections showing bedding and fault orientation in gray and black, respectively. Orientation of slip indicators are given as pole projections with arrows indicating sense of slip.

3.2. Thrusts and Strike-Slip Faults in the Eastern Jura Mountains

The eastern Jura Mountains are marked by closely spaced thrust faults along which the basal décollement crops out at the surface. The Mesozoic sedimentary succession exposed in the hanging wall of the thrusts generally dips gently to the south (Malz et al., 2016). We collected samples from four locations (see Figure 2): Slickenfibres from two thrust faults within the upper Muschelkalk Group (Schinznach Formation, Middle Triassic) at the locations Habsburg (HB; 47.46305°N, 8.18160°E; Figures 4a and 4b) and Asp-Ueslimatt (AU; 47.44605°N, 8.05435°E; Figure 4c) and slickenfibres from two subvertical strike-slip faults within the Dogger Group (Hauptrogenstein, Middle Jurassic) at the locations Aaretal-Auenstein (AA; 47.42466°N, 8.15890°E; Figure 4d) and Asperchus (AK; 47.42525°N, 8.05430°E; Figures 4e and 4f). The sampled HB and AU thrusts dip gently to the south, almost parallel to the bedding (Figures 4a and 4c). While a direct connection of these thrust faults to the basal décollement (such as is clear at the

SHA thrust) is not evident, their relation to deformation along it is given due to their kinematic compatibility with NNW-SSE shortening which prevailed during the main phase of Jura thrusting in this area (Becker, 2000; Madritsch, 2015). The sampled AA and AK strike-slip faults are typical for the eastern Jura Mountains and also constrain NNW-SSE shortening in relation to the formation of the Jura fold-and-thrust belt (Madritsch, 2015). Both cut subvertically through Middle Jurassic limestones and strike roughly N-S (Figures 4d and 4e). The centimeter thick slickenfibers on these fault planes indicate sinistral movement (Figure 4f), also being compatible with Miocene NNW-SSE shortening (Becker, 2000; Madritsch, 2015). The strike-slip slickenfibers are oriented parallel to the bedding and dip gently to the south which was previously interpreted as tilting due to thrust-related folding postdating calcite precipitation and strike-slip faulting (Madritsch, 2015).

4. Analytical Methods

4.1. Calcite U-Pb LA-ICP-MS Dating

Calcite U-Pb dating was performed by laser ablation inductively coupled plasma mass spectrometry (LA-ICP-MS) on polished thick sections (60 μm) and chips mounted in epoxy at ETH Zurich using an ASI RESOLUTION S-155, excimer (ArF, 193 nm) laser ablation system coupled to a Thermo Element XR sector-field ICP-MS. The analytical method and correction procedure follow Roberts et al. (2017) using NIST 614 and WC-1 as primary reference materials and Guillong et al. (2020) using a matched ablation crater aspect ratio for the primary reference materials and unknowns (in this study, spot sizes of 110 and 163 μm and repetition rates of 5.0 and 7.4 Hz, respectively, depending on the U content). In addition to the primary reference materials and samples, the secondary reference materials JT and ASH-15D (Guillong et al., 2020; Nuriel et al., 2020) were analyzed in each session to assess accuracy and repeatability. Correction for matrix effects with WC-1 was done by anchoring to a value of 0.85 common-lead, while samples and secondary reference materials were not anchored. No disequilibrium correction was applied. U-Pb ages were calculated from Tera-Wasserburg concordia lower intercepts using the IsoplotR software package (Vermeesch, 2018). All uncertainties are reported at the 95% confidence level. A long-term excess variance of 2.5% relative was propagated by quadratic addition to the uncertainty of the individual, lower intercept dates (Guillong et al., 2020). Prior to and after the LA-ICP-MS measurements, cathodoluminescence microscopy was conducted in order to identify potential growth zonings and to identify misplaced or defective ablation spots which were then excluded from the data. In addition to this, the lower intercept dates with a MSWD value >4.3 or an absolute uncertainty >2 Ma were not considered. More details on the analytical methods can be found as supporting information.

4.2. Clumped Isotope Thermometry

For clumped isotope analyses, 1–2 mg of calcite powder per sample was obtained by drilling with a hand-held drill at low RPM and homogenized with a mortar and pestle. Mineralogy was checked by XRD prior to analysis to avoid carbonate mixtures. Clumped isotope measurements were conducted at ETH Zurich using a Thermo Scientific Kiel IV carbonate device coupled to a Thermo Scientific MAT253 isotope ratio mass spectrometer (IRMS) based on the methods described by Meckler et al. (2014) and Müller et al. (2017). In addition to the removal of water and noncondensable gases by the Kiel IV carbonate device, potential isobaric contaminations were removed by a Porapak Q resin held at -40 °C. Backgrounds on m/z 44–47 were determined at the beginning of each analytical session by high-voltage peak scans at five different intensities between 10 and 30 V (Bernasconi et al., 2013). Data reduction were carried out with the Easotope software package (John & Bowen, 2016). Normalization and projection of clumped isotope measurements into the carbon dioxide equilibrium scale (CDES) was done using the carbonate standards ETH-1, ETH-2, and ETH-3 with the values of (Bernasconi et al., 2018). Δ_{47} temperatures were calculated with the recalculated Kele et al. (2015) calibration (Bernasconi et al., 2018) and $\delta^{18}\text{O}_{\text{fluid}}$ was calculated using the calibration of (Kim & O'Neil, 1997). Measurements failing outlier tests and with a deviation from the median Δ_{47} value of the sample of $\geq 0.090\text{‰}$ (2% of all measurements) were not considered. Errors in Δ_{47} temperatures are reported at the 95% confidence level (Fernandez et al., 2017).

5. Results

5.1. Structural Analysis

At the SHA thrust, secondary calcites in veins pervading the cataclastic fault breccia and the outer damage zone of the thrust's footwall show syntaxial, elongated blocky and blocky textures (e.g., Figure 5e). Based on structural observations (crosscutting relationships and vein orientations), we initially differentiated between four populations of calcite veins in the footwall of the SHA thrust (VP1-VP4, from old to young; Figures 3b and 5). Veins of VP1 (blue) are thin and crosscut by VP2 veins (orange) while exhibiting various dips. Veins of VP2 in the outer damage zone mostly show subhorizontal orientations. Within the fault breccia, VP2 veins often show brittle deformation themselves (truncated at clast boundaries; Figures 5b and 5e) and structurally predate the thrust-related cataclasis. In the outer damage zone, these veins are occasionally associated with dip-slip slickenfibers indicating thrust kinematics. Veins of VP3 (green) are found exclusively within the fault breccia and differ from VP2 in overprinting the cataclastic fabric by cutting through multiple clasts. Thus, they formed syncataclasis or postcataclasis. Veins of VP4 (pink) show subvertical orientations and cut through veins of VP1 to VP3. As the Schafisheim cores are nonoriented, the azimuth of these veins remains unknown.

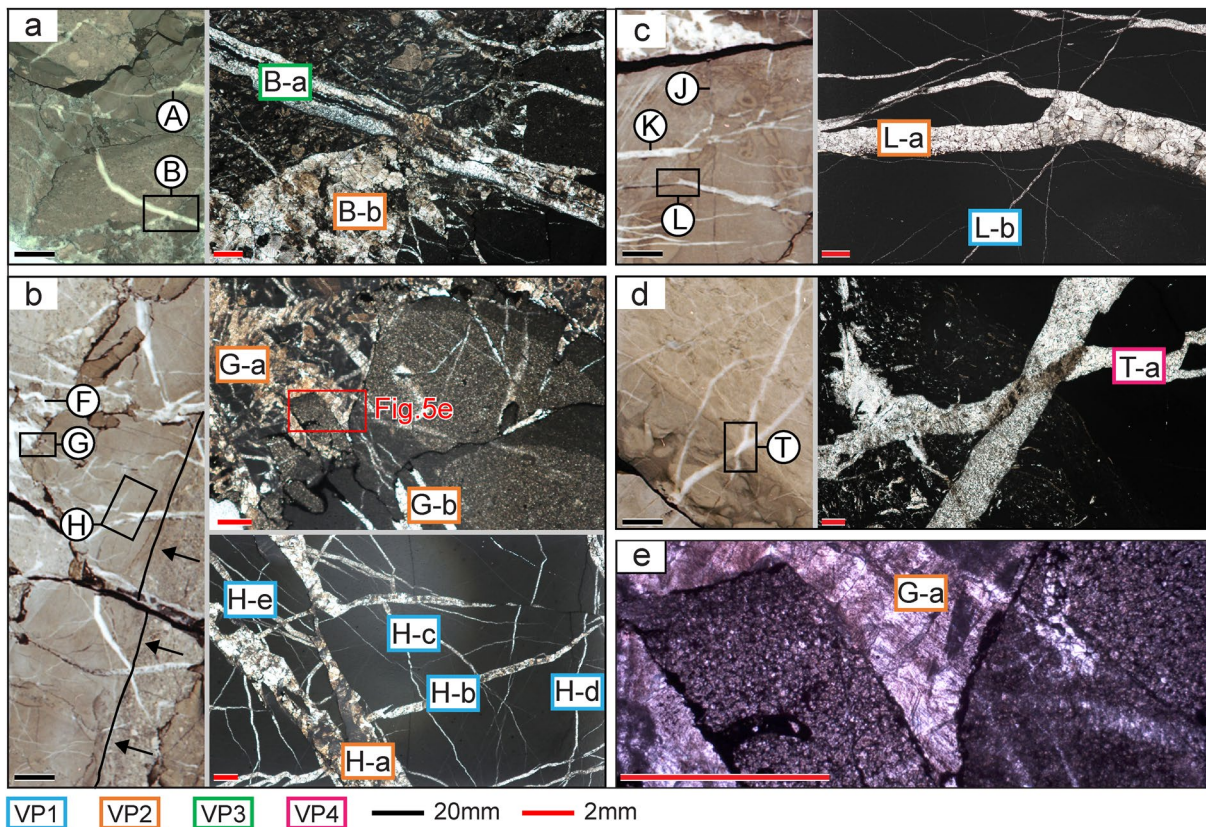


Figure 5. Core photographs with black squares indicating the location of thin-section images on the right. Scale bars indicate 20 mm (black) and 2 mm (red). (a) VP3 veins (A, B-a) overprint the cataclastic texture of the fault breccia by cutting through multiple clasts and a VP2 vein (B-b). (b) Fault breccia with rotated clasts indicated by a subvertical sedimentary bedding plane (black line marked by arrows). The magnified sections show the cataclastic overprint of VP2 veins (G-a and G-b) being truncated at clast boundaries and VP1 veins being crosscut by VP2 veins (e.g., H-a vs. H-b and H-e). (c) VP2 veins in the outer damage zone with the original subhorizontal orientation and a VP1 vein (L-b) being crosscut by a VP2 vein (L-a). (d) Subvertical VP4 vein crosscutting an earlier vein of unknown age. (e) Truncation of a VP2 vein at a clast boundary (G-a, indicated by a red square in Figure 5b) under a transmitted light microscope.

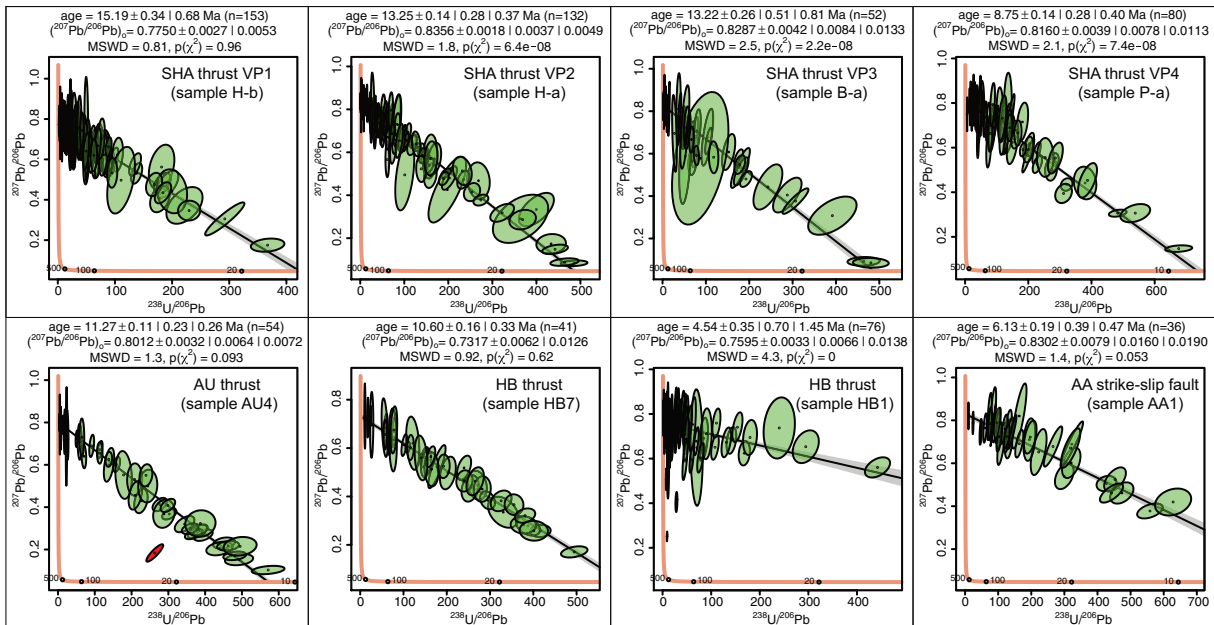


Figure 6. Tera-Wasserburg concordia diagrams of a representative subset of samples covering all observed deformation intervals.

5.2. Calcite U-Pb LA-ICP-MS Analysis

A total of 45 vein calcites yielded reliable age data. A selection of Tera-Wasserburg concordia diagrams of a representative subset of samples covering all observed deformation intervals is shown in Figure 6 and the complete set of Tera-Wasserburg plots can be found as supporting information.

For the SHA thrust, the individual ages of veins across all populations range between 15.2 ± 0.8 and 8.8 ± 0.5 Ma (Figure 8 and supporting information). An average age of each population was determined as the weighted mean considering the uncertainties of the individual vein ages. This averaging is justified by the fact that the vein populations are structurally constrained to correspond to different deformation phases and provides a more robust constraint of the timing of each deformation phase. VP1 yielded a resulting weighted mean age of 14.3 ± 0.5 Ma ($n = 9$). The weighted means of individual vein ages for VP2 and VP3 are indistinguishable from each other, with a mean age of 13.2 ± 0.2 Ma obtained when pooled together (VP2 and VP3, $n = 21$). VP4 shows a weighted mean age of 9.1 ± 1.4 Ma ($n = 3$). We note that, although some of the individual ages of the two vein populations overlap within uncertainties, the offset between the average ages of VP1 and those of VP2 and VP3 is statistically significant, by minimum 0.5 Ma and maximum 1.7 Ma when considering uncertainties at the 95% confidence level (CL).

For the outcrops in the eastern Jura Mountains, the reported U-Pb ages correspond to single dates of individual samples. Because of the limited number of samples and the large spread of ages, no weighted means were calculated. The slickenfibers from the AU thrust yielded four U-Pb ages between 11.3 ± 0.9 and 9.9 ± 0.6 Ma. The slickenfibers from the HB thrust plot in two groups with significantly different ages: A first group with four ages ranging from 10.6 ± 0.4 to 8.0 ± 0.6 Ma and a second group with two ages of 5.7 ± 0.7 and 4.5 ± 1.5 Ma, respectively. The sample from the AK strike-slip fault yielded an age of 9.3 ± 1.1 Ma and the sample from the AA strike-slip fault of 6.1 ± 0.5 Ma, respectively. The age data of the AK strike-slip fault is in good agreement with the only other reported calcite slickenfiber U-Pb age of 9.1 ± 0.9 Ma, stemming from a similar structural feature in the Jura Mountains ~ 25 km west of Schafisheim (Madritsch, 2015; Rittner, 2013).

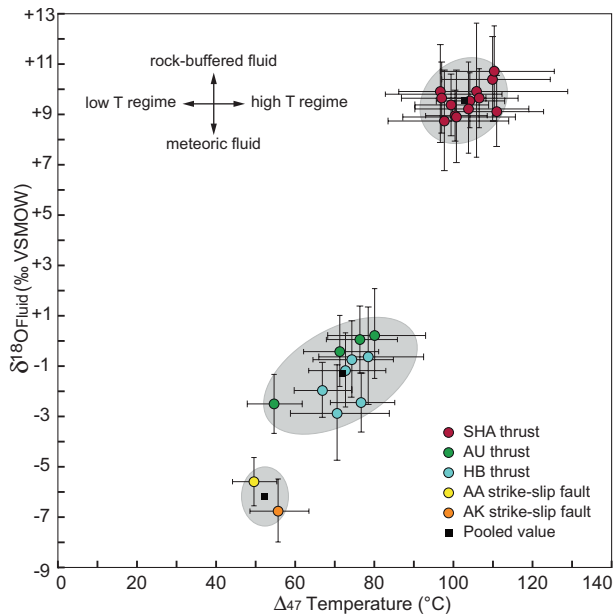


Figure 7. Clumped isotope data plotted as Δ_{47} temperature vs. $\delta^{18}\text{O}_{\text{fluid}}$ with the error bars showing 95% confidence intervals (see text for discussion).

5.3. Clumped Isotope Analysis

A total of 300 measurements on a subset of 25 samples with reliable age data and covering the entire time span of recorded deformation were considered for the reconstruction of clumped isotope temperatures (Δ_{47}) and the oxygen isotope composition of the precipitating fluids ($\delta^{18}\text{O}_{\text{fluid}}$). A table with all data can be found as supporting information and the entire data set including the carbonate standards is available as Easotope Database. When plotted as Δ_{47} temperature vs. $\delta^{18}\text{O}_{\text{fluid}}$, the data from the different sites and fault types group in fields reflecting three distinct burial settings at the time of faulting (Figure 7).

For the SHA thrust, the Δ_{47} temperatures and $\delta^{18}\text{O}_{\text{fluid}}$ compositions of the four vein populations are indistinguishable from each other at the 95% CL (Figure 7) and pooled together yielded a Δ_{47} temperature of $104 \pm 3 \text{ }^\circ\text{C}$ and a $\delta^{18}\text{O}_{\text{fluid}}$ of $+9.5 \pm 0.4\text{‰}$, VSMOW. The samples from the AU and HB thrusts overlap in most cases in both Δ_{47} temperatures and $\delta^{18}\text{O}_{\text{fluid}}$ at the 95% CL (Figure 7) and therefore were also pooled together (AU and HB) yielding a Δ_{47} temperature of $73 \pm 3 \text{ }^\circ\text{C}$ and a $\delta^{18}\text{O}_{\text{fluid}}$ of $-1.3 \pm 0.5\text{‰}$, VSMOW. The same procedure was applied for the AK and AA strike-slip faults (AK and AA) yielding a pooled Δ_{47} temperature of $53 \pm 4 \text{ }^\circ\text{C}$ and a $\delta^{18}\text{O}_{\text{fluid}}$ of $-6.2 \pm 0.8\text{‰}$, VSMOW.

6. Discussion

6.1. Timing of Deformation

Figure 8 shows a compilation and interpretation of the U-Pb data from the SHA thrust. At Schafisheim, VP1 veins dated at $14.3 \pm 0.5 \text{ Ma}$ on average are the earliest evidence for brittle deformation in the thrust's footwall and accordingly, for tectonic activity of the basal décollement. Besides being overprinted by cataclasis related to thrusting, a direct kinematic relation of VP1 to the thrust is not fully constrained but is plausible for two reasons. First, VP1 veins are restricted to the damage zone in the footwall of the thrust. Second, clumped isotopes show that they formed under very similar temperature conditions to the other populations with well-established structural relations to the thrust. Therefore, we infer VP1 to be related to Alpine shortening, representing the minimum age for its onset. Unambiguous evidence for a phase of thrusting at Schafisheim at $13.2 \pm 0.2 \text{ Ma}$ is provided by the pooled VP2 and VP3. The fact that VP2 and VP3 yield identical U-Pb ages while showing different structural relationships (VP2 being overprinted by the cataclastic fabric and VP3 overprinting the same) gives excellent constraints on the timing of cataclasis in the thrust's footwall. The subvertical VP4 veins dated at $9.1 \pm 1.4 \text{ Ma}$ on average clearly post-date the thrust-related cataclasis at the SHA thrust (Figure 8).

Figure 9 shows a compilation of the U-Pb data from all sample locations and fault types presented in Figure 2. Evidently, the thrusts and strike-slip faults from the eastern Jura Mountains constrain younger phases of foreland deformation between 11.3 ± 0.4 and $4.5 \pm 1.5 \text{ Ma}$ implying a duration of thrusting activity of at least $\sim 10 \text{ Ma}$ (14.3–4.5 Ma). While the youngest recorded deformation phase at Schafisheim is at $9.1 \pm 1.4 \text{ Ma}$, deformation records in the adjacent Jura Mountains are as young as $4.5 \pm 1.5 \text{ Ma}$. Notably, thrusting occurred simultaneously with strike-slip faulting. Moreover, strike-slip faulting initiated prior to large-scale folding in the Jura Mountains as evident from tilted strike-slip slickenslides (e.g., at the AK strike-slip fault; Madritsch, 2015). Accordingly, folding in this area must have occurred after $9.3 \pm 1.1 \text{ Ma}$ ago. Worth mentioning is that the steeply dipping VP4 veins at Schafisheim with U-Pb ages similar to the AK strike-slip fault predate thrust-related folding in the Jura Mountains.

The observed time lag of 3 Ma between the reconstructed onsets of deformation at the SHA thrust (14.3 Ma) and in the Jura Mountains (11.3 Ma) might indicate a foreland-directed thrust propagation signal (Figure 9). However, the U-Pb data need to be interpreted with caution in this regard, because of the spatially

limited coverage of the available samples. In other words, potential older deformation in other locations in the Jura Mountains may have been missed. Similarly, the oldest ages from the SHA thrust should be regarded as a minimum age for the onset of tectonic activity along the basal décollement and it is possible that deformation initiated even earlier. Also, it is important to keep in mind that any motion of the thin-skinned foreland thrust system more distal than Schafisheim must also occur at the basal décollement of Schafisheim to some extent, even if not recorded by the analyzed veins in the footwall of SHA thrust.

Despite the above-mentioned caveats, our data from the Schafisheim well clearly constrain that deformation along the basal décollement already started in Langhian times (16–13.8 Ma) at the latest. This is earlier than commonly inferred for the Jura Mountains (late Serravallian or later; Becker, 2000; Kälin, 1997; Madritsch, 2015; Malz et al., 2016; Rittner, 2013; Sommaruga et al., 1995; Ziegler & Fraefel, 2009) and corroborates isolated field observations of early stage foreland shortening close to the Alpine front already during Burdigalian times (Beck et al., 1998; Deville et al., 1994; Pfiffner, 2014). The maximum age for the main phase of thrust-related folding in the eastern Jura Mountains of 9.3 Ma, constrained by the tilted AK strike-slip fault, is in good agreement with previous estimates for the timing of deformation in that area (Becker, 2000; Malz et al., 2016). The youngest age constraints for thrusting obtained in this study (4.5 Ma at the HB thrust) are well in line with previous estimates for the termination of thin-skinned deformation (Madritsch et al., 2008; Ustaszewski & Schmid, 2007). Combining our data with the existing biostratigraphic age constraints from different locations in the foreland suggests that the decoupling and thrusting along the basal décollement initiated at ~20–16 Ma close to the Alpine front (Beck et al., 1998; Deville et al., 1994; Pfiffner, 2014) and was followed by foreland-directed propagation of deformation toward the distal Molasse

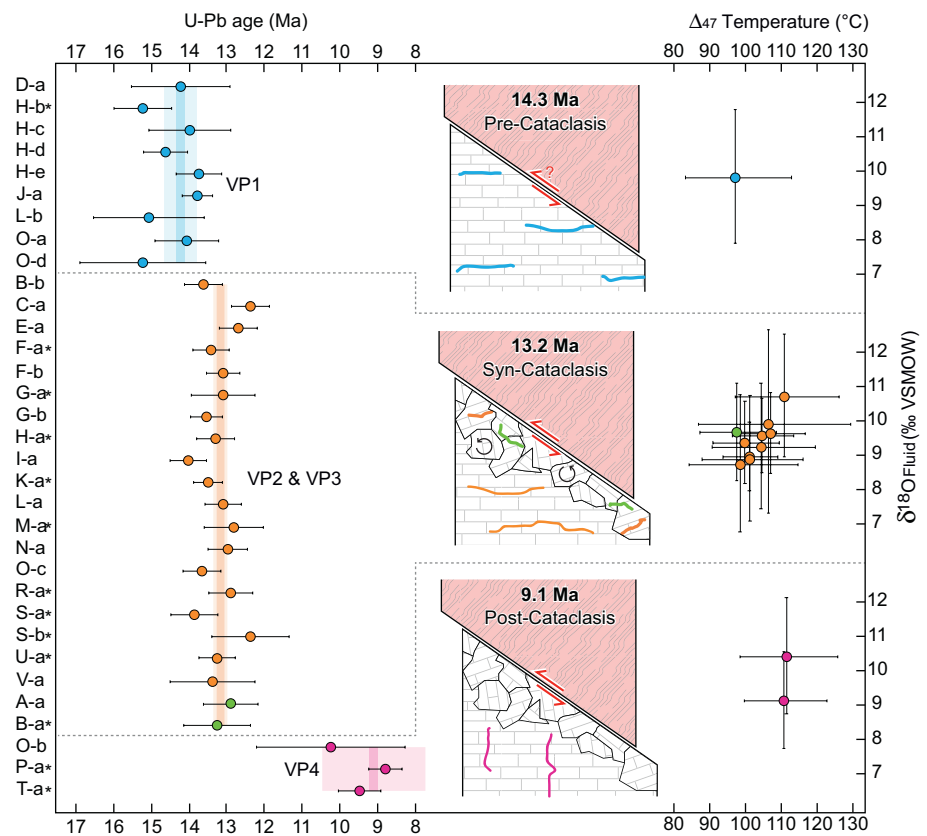


Figure 8. Reconstruction of the SHA thrust evolution and related vein formation with U-Pb and clumped isotope data. Colors correspond to vein populations (VP1 in blue, VP2 in orange, VP3 in green, and VP4 in pink) as in Figures 3b and 5. Letters on the left side refer to the veins as in Figure 5 and in the Tera-Wasserburg isochron diagrams and sample images in the supporting information. Veins analyzed for clumped isotopes are indicated with stars. Error bars show 95% confidence levels for both clumped isotope and individual U-Pb data of calcite veins. Dark shaded lines show the weighted mean U-Pb age and the lighter shading the uncertainty at the 95% confidence level for each vein population.

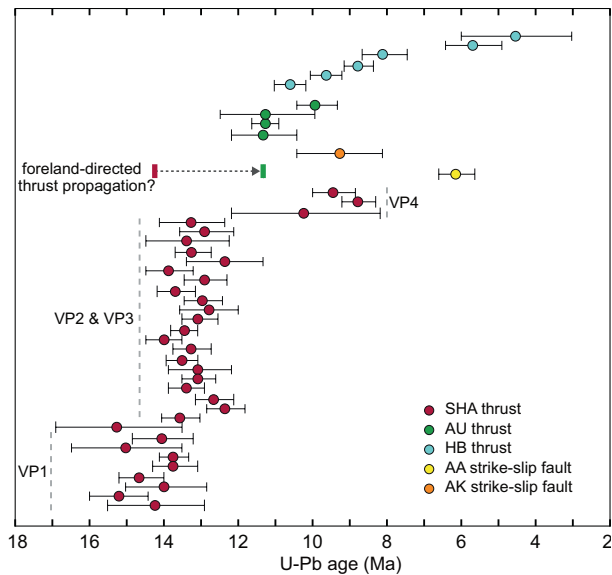


Figure 9. U-Pb data from the different sites arranged as a S-N transect. Error bars show 95% confidence levels.

Basin at Schafisheim (initiating at 14.3 Ma at the latest, this study), to the Internal Jura Mountains (initiating at 11.3 Ma at the latest, this study), and to the frontal thrusts (initiating only after ~11-9 Ma; Becker, 2000; Kälin, 1997 and references therein).

The indications for early stage thrusting at Schafisheim predate thermochronologically constrained thrust pulses between 10 and 5 Ma in the Subalpine Molasse of the more proximal foreland (Figures 1a and 1b; Von Hagke et al., 2012). This may imply an initial backward breaking sequence of foreland thrusting across the northwestern Alpine foreland as suggested for the Subalpine Molasse further to the east (Ortner et al., 2015). However, the same authors mention that stratigraphic data suggests tectonic activity in this region before 12 Ma. The younger pulses of deformation between 11.3 ± 0.4 and 4.5 ± 1.5 Ma in our area of investigation corresponds very well with the timing of shortening in the Subalpine Molasse between 10 and 5 Ma (Von Hagke et al., 2012) and in the Central Alps starting at 13-12 Ma (Herwegh et al., 2019). This proves simultaneous tectonic activity along both thrust fronts; e.g., the Jura Mountains and the Subalpine Molasse over a time span of several million years as suggested by Von Hagke et al. (2012).

6.2. Temperatures and Fluid Flow During Deformation

Figure 10 shows the clumped isotope data plotted against the corresponding U-Pb ages measured on the same samples. Contemporaneous deformation recorded at different locations during the time interval between 11.3 ± 0.4 and 8.0 ± 0.6 Ma allows for a direct comparison of the deformation temperatures and syntectonic fluid flow between the different burial settings (the distal Molasse Basin vs. the Jura Mountains) and fault types (thrusts vs. strike-slip faults). At the SHA thrust, the pooled $\delta^{18}\text{O}_{\text{fluid}}$ of $+9.5 \pm 0.4\text{‰}$ (VSMOW) indicate precipitation from a parent fluid modified by extensive fluid-rock interaction at high temperatures. Equilibration of a fluid with the host rock, for which we measured a $\delta^{18}\text{O}$ of -5.94‰ (VPDB), at 104 °C will result in a $\delta^{18}\text{O}_{\text{fluid}}$ of $+9.1\text{‰}$ (VSMOW). The consistency of the recorded $\delta^{18}\text{O}_{\text{fluid}}$ with the expected values for equilibrium shows that the vein calcites at the SHA thrust precipitated from a fluid in or near equilibrium with the host rock. Therefore, the vein calcites reflect ambient burial temperatures during times of faulting. Because of the equilibration of the oxygen isotope composition with the host rock, the calculated $\delta^{18}\text{O}_{\text{fluid}}$ does not indicate its origin. Thus, it remains open if the fluid sourced from greater depth and migrated upwards along the thrust fault or if it originally was of meteoric origin and infiltrated from the overlying units. In either case, the flow rate was low enough for thermal and oxygen isotopic equilibration with the host rock.

Compared to the SHA thrust, the AU and HB thrusts with a pooled Δ_{47} temperature of $73 \pm 3\text{ °C}$ and a pooled $\delta^{18}\text{O}_{\text{fluid}}$ of $-1.3 \pm 0.5\text{‰}$ (VSMOW) imply significantly less overburden at the time of faulting in the Jura Mountains. This difference is interpreted to reflect the northward decreasing thickness of Molasse deposits. A fluid in equilibrium with the host rock at the AU and HB thrusts with a $\delta^{18}\text{O}$ of -5.62‰ and a temperature of 73 °C would have a $\delta^{18}\text{O}_{\text{fluid}}$ of $+5.2\text{‰}$ (VSMOW), much more enriched in ^{18}O than the -1.3‰ observed. There are two scenarios to explain this observation. Based on our data, both scenarios are possible and for both cases, we argue that the 73 °C recorded by the slickenfiber calcites approximate the ambient temperatures during times of faulting at the AU and HB thrusts. In the first scenario, meteoric fluids infiltrated from the overlying units and in absence of other fluids were heated up while only partially equilibrating in oxygen isotopes with the host rock and maintaining some of the original isotopically light meteoric water signatures. This scenario implies that these thrusts were connected to the surface or shallow groundwater aquifers. As thermal equilibration takes place much faster than oxygen isotope exchange, a fluid with a substantial modification of its original oxygen isotope composition due to water-rock interaction will reach the same temperature as the host rock. In the second scenario, deep-seated hot fluids rapidly ascended along the fault zone, e.g., during earthquakes, and mixed with colder pore waters, as was

shown in an active fault in the Apennines (Smeraglia et al., 2018). This scenario is consistent with evidence for fluid flow along the crystalline basement and/or the lowermost sedimentary unit, the Bundsandstein Group (Figure 3), sourcing from infiltration of meteoric waters in the Black Forest highland (Figure 1) and ascending into the lower Mesozoic formations along cross-formational faults in the northeastern Swiss Molasse Basin (Aschwanden et al., 2019). As the difference in burial between the basal décollement and the crystalline basement is only minor (e.g., some >50 m at Schafisheim, see Figure 3) and since fluid flow most likely was concentrated in the permeable weathering zone of the basement and/or the lowermost sedimentary unit, the ascending fluids were only few degrees warmer than ambient burial temperatures at the basal décollement. Moreover, the local extent of the AU and HB thrusts with no large-scale network of veins speak against a rapid fluid ascend so that, if sourcing from greater depth, the ascending fluids would have thermally equilibrated with the host rock.

A maximum value for the $\delta^{18}\text{O}$ of the unmodified meteoric endmember (e.g., before interaction with the host rocks during infiltration) is provided by the AA and AK strike-slip faults showing the most depleted oxygen isotope signatures of $-6.2 \pm 0.8\text{‰}$ (VSMOW) when pooled together. Compared to this value, the reconstructed fluids from the AU and HB thrusts are about 5‰ enriched. During the time needed for this enrichment, temperatures will have fully equilibrated. Accordingly, we consider the Δ_{47} temperatures from the AU and HB thrusts as close approximation for the ambient temperatures during deformation at the basal décollement in the region of the present-day eastern Jura Mountains. The AA and AK strike-slip faults show a colder pooled Δ_{47} temperature of $53 \pm 4\text{ °C}$ and much more meteoric $\delta^{18}\text{O}_{\text{fluid}}$ signatures compared to the AU and HB thrusts. To some extent, this may be due to the location of these faults, ~400 m higher in the stratigraphic column (Middle Jurassic Hauptrogenstein vs. Middle Triassic Schinznach Fm.). Furthermore, the steepness of the strike-slip faults has likely favored meteoric water infiltration at higher rates resulting in less water-rock interaction. Therefore, the $53 \pm 4\text{ °C}$ recorded by the slickenfibers could be lower than the ambient burial temperatures.

Since the SHA thrust as well as the AU and HB thrusts are located close to the basal décollement and underwent thermal equilibration with the host rocks, the Δ_{47} temperatures of the vein calcites constrain deformation within the décollement during basal thrusting. The temperature difference of 30 °C between the interior of the distal Molasse Basin and the present-day Jura Mountains along the basal décollement correlates with distinct microfabrics of anhydrite mylonites defining deformation regimes of temperature and deformation mechanisms (Jordan, 1992). Thermal equilibrium at the SHA, HB, and AU thrusts allows for estimations of deformation depths. Assuming a geothermal gradient between 20 °C km^{-1} (Mazurek

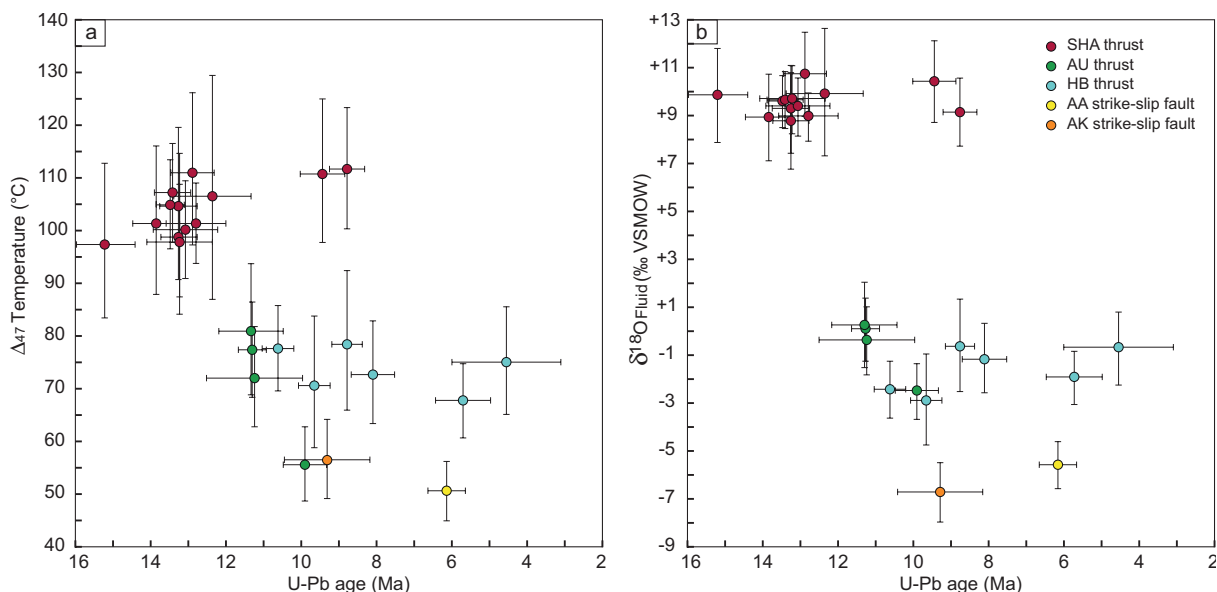


Figure 10. (a) Δ_{47} temperatures and (b) $\delta^{18}\text{O}_{\text{fluid}}$ of the vein calcites plotted against their corresponding U-Pb ages.

et al., 2006) and $30\text{ }^{\circ}\text{C km}^{-1}$ (Cederbom et al., 2004) during Mid-Late Miocene times and a temperature of the infiltrating meteoric fluids of $10\text{ }^{\circ}\text{C}$ (modern temperature of springs in the Jura Mountains, Jeannin et al., 2016), thrusting took place under 3.1–4.7 km of sedimentary overburden at Schafisheim and under 2.1–3.1 km in the eastern Jura mountains, respectively.

Widely constant Δ_{47} temperatures and $\delta^{18}\text{O}_{\text{fluid}}$ over time indicates deformation under constant burial conditions (Figure 10). Accordingly, the analyzed faults did not experience significant exhumation either through piggy-back transport along the shallow dipping décollement or erosion of the overlying sediments or further burial between 14.3 and 4.5 Ma. This has implications for the amount and onset of erosion during the late-stage evolution of the Molasse Basin and confirms apatite fission track data suggesting initiation of major erosion in the northwestern Alpine foreland at ~ 5 Ma (Cederbom et al., 2004, 2011; Kuhlemann & Kempf, 2002). Based on the calculated sedimentary overburden during thrusting, we estimate 2.0–3.6 km of erosion at Schafisheim since Pliocene times. This value is in the range of other estimates for erosion of the undeformed Molasse in Switzerland of 1 km (Mazurek et al., 2006; assumed geothermal gradient of $\leq 20\text{ }^{\circ}\text{C km}^{-1}$), 2–2.6 km (Schegg et al., 1997; assumed geothermal gradient of $30\text{ }^{\circ}\text{C km}^{-1}$), 1.4–3.5 km (Cederbom et al., 2004; assumed geothermal gradient of $20\text{--}30\text{ }^{\circ}\text{C km}^{-1}$) and 0.7–1.8 km (Cederbom et al., 2011; assumed geothermal gradient of $25\text{--}37\text{ }^{\circ}\text{C km}^{-1}$) based on vitrinite reflectance and apatite fission tracks data.

7. Conclusion

The combined carbonate U-Pb and clumped isotope data presented here provide the first absolute age and temperature constraints for deformation along the basal décollement of the Jura Mountains, a classical example for a thin-skinned foreland fold-and-thrust belt and allows to draw four major conclusions. (1) The age data from the distal Molasse Basin at Schafisheim shows that thrusting along the basal décollement was active earlier than commonly inferred for the Jura Mountains, already at Langhian times. (2) The associated deformation was not a short-lived event but occurred over a time period between at least 14.3 and 4.5 Ma with contemporaneous activity (and potential interplay) of thrusts and strike-slip faults in the Jura Mountains. (3) Over this time period, the burial conditions remained constant showing that large-scale erosion of the Molasse Basin at its northern margin did not initiate before 4.5 Ma. (4) The reconstructed temperatures and fluid compositions show an increase in burial of the basal décollement from north to south, reflecting different amounts of Molasse overburden and provide constraints for in-situ temperatures during deformation and syntectonic fluid flow. Beyond, our study demonstrates the great potential of combined carbonate U-Pb geochronology and clumped isotope thermometry for reconstructing the absolute timing as well as the temperatures and fluids involved in foreland thrust systems and provides perspectives for further studies.

Data Availability Statement

All new data presented in this article are available to the public at the data sharing infrastructure of EarthChem (Looser et al., 2021; <https://ecl.earthchem.org/view.php?id=1824>; DOI: 10.26022/IEDA/111824).

Acknowledgments

The authors thank the Swiss National Cooperative for the Disposal of Radioactive Waste (Nagra) for access to the Schafisheim cores. This study was funded by the Swiss National Science Foundation project number 200021_169849. The authors thank the Associate Editor, Djordje Grujic and the two reviewers Perach Nuriel and David Hindle for their constructive comments that helped to improve the manuscript. This work also benefited from comments by Adrian Piffner, Christoph von Hagke, and Uwe Ring on an earlier manuscript version.

References

- Aschwanden, L., Diamond, L. W., Mazurek, M., & Davis, D. W. (2019). Creation of secondary porosity in dolostones by upwelling basement water in the foreland of the Alpine orogen. *Geofluids*, 2019, 5210404. <https://doi.org/10.1155/2019/5210404>
- Beaudoin, N., Lacombe, O., Roberts, N. M. W., & Koehn, D. (2018). U-Pb dating of calcite veins reveals complex stress evolution and thrust sequence in the Bighorn Basin, Wyoming, USA. *Geology*, 46, 1015–1018. <https://doi.org/10.1130/G45379.1>
- Beck, C., Deville, E., Blanc, E., Philippe, Y., & Tardy, M. (1998). Horizontal shortening control of middle miocene marine siliciclastic accumulation (upper Marine Molasse) in the Southern Termination of the Savoy Molasse Basin (northwestern Alps/southern Jura) (Vol. 134, pp. 263–278). Geological Society Special Publication. <https://doi.org/10.1144/GSL.SP.1998.134.01.12>
- Becker, A. (2000). The Jura Mountains—An active foreland fold-and-thrust belt? *Tectonophysics*, 321, 381–406. [https://doi.org/10.1016/S0040-1951\(00\)00089-5](https://doi.org/10.1016/S0040-1951(00)00089-5)
- Bergman, S. C., Huntington, K. W., & Crider, J. G. (2013). Tracing paleofluid sources using clumped isotope thermometry of diagenetic cements along the Moab fault, Utah. *American Journal of Science*, 313, 490–515. <https://doi.org/10.2475/05.2013.03>
- Bernasconi, S. M., Hu, B., Wacker, U., Fiebig, J., Breitenbach, S. F. M., & Rutz, T. (2013). Background effects on Faraday collectors in gas-source mass spectrometry and implications for clumped isotope measurements. *Rapid Communications in Mass Spectrometry*, 27, 603–612. <https://doi.org/10.1002/rcm.6490>

- Bernasconi, S. M., Müller, I. A., Bergmann, K. D., Breitenbach, S. F. M., Fernandez, A., Hodell, D. A., et al. (2018). Reducing uncertainties in carbonate clumped isotope analysis through consistent carbonate-based standardization. *Geochemistry, Geophysics, Geosystems*, 19, 2895–2914. <https://doi.org/10.1029/2017GC007385>
- Bolliger, T., Engesser, B., & Weidmann, M. (1993). Première découverte de mammifères pliocènes dans le Jura neuchâtelois. *Eclogae Geologicae Helvetiae*, 86, 1031–1068.
- Burkhard, M. (1990). Aspects of the large-scale Miocene deformation in the most external part of the Swiss Alps (Subalpine Molasse to Jura fold belt). *Eclogae Geologicae Helvetiae*, 83, 559–583.
- Burkhard, M., & Sommaruga, A. (1998). Evolution of the Western Swiss Molasse Basin: Structural relations with the Alps and the Jura Belt (Vol. 134, pp. 279–298). Geological Society Special Publication. <https://doi.org/10.1144/GSL.SP.1998.134.01.13>
- Buxtorf, A. (1907). Zur Tektonik des Kettenjura. *Berichte über die Versammlungen des Oberrheinischen geologischen Vereins*, 40, 79–111.
- Cederbom, C. E., Sinclair, H. D., Schlunegger, F., & Rahn, M. K. (2004). Climate-induced rebound and exhumation of the European Alps. *Geology*, 32, 709–712. <https://doi.org/10.1130/G20491.1>
- Cederbom, C. E., Van Der Beek, P., Schlunegger, F., Sinclair, H. D., & Oncken, O. (2011). Rapid extensive erosion of the North Alpine foreland basin at 5–4Ma. *Basin Research*, 23, 528–550. <https://doi.org/10.1111/j.1365-2117.2011.00501>
- Deville, E., Blanc, E., Tardy, M., Beck, C., Cousin, M., & Ménard, G. (1994). Thrust propagation and syntectonic sedimentation in the Savoy Tertiary Molasse basin (Alpine foreland). In A. Mascle (Ed.), *Hydrocarbon and petroleum geology of France* (Vol. 4, pp. 269–280). Berlin: Springer. https://doi.org/10.1007/978-3-642-78849-9_19
- Fernandez, A., Müller, I. A., Rodríguez-Sanz, L., van Dijk, J., Looser, N., & Bernasconi, S. M. (2017). A reassessment of the precision of carbonate clumped isotope measurements: Implications for calibrations and paleoclimate reconstructions. *Geochemistry, Geophysics, Geosystems*, 18, 4375–4386. <https://doi.org/10.1002/2017GC007106>
- Guillong, M., Wotzlaw, J., Looser, N., & Laurent, O. (2020). Evaluating the reliability of U–Pb laser ablation inductively coupled plasma mass spectrometry (LA-ICP-MS) carbonate geochronology: Matrix issues and a potential calcite validation reference material. *Geochronology*, 2, 155–167. <https://doi.org/10.5194/gchron-2-155-2020>
- Herwegh, M., Berger, A., Glotzbach, C., Wangenheim, C., Mock, S., Wehrens, P., et al. (2019). Late stages of continent-continent collision: Timing, kinematic evolution, and exhumation of the northern rim (Aar Massif) of the Alps. *Earth-Science Reviews*, 200, 102959. <https://doi.org/10.1016/j.earscirev.2019.102959>
- Huntington, K. W., & Lechler, A. R. (2015). Carbonate clumped isotope thermometry in continental tectonics. *Tectonophysics*, 647–648, 1–20. <https://doi.org/10.1016/j.tecto.2015.02.019>
- Jeannin, P. Y., Hessenauer, M., Malard, A., & Chapuis, V. (2016). Impact of global change on karst groundwater mineralization in the Jura Mountains. *Science of the Total Environment*, 541, 1208–1221. <https://doi.org/10.1016/j.scitotenv.2015.10.008>
- John, C. M., & Bowen, D. (2016). Community software for challenging isotope analysis: First applications of ‘Easotope’ to clumped isotopes. *Rapid Communications in Mass Spectrometry*, 2285–2300. <https://doi.org/10.1002/rcm.7720>
- Jordan, P. (1992). Evidence for large-scale decoupling in the Triassic evaporites of northern Switzerland: An overview. *Eclogae Geologicae Helvetiae*, 85, 677–693.
- Jordan, P., Malz, A., Heuberger, S., Pietsch, J., Kley, J., & Madritsch, H. (2015). *Regionale geologische Profile durch die Nordschweiz und 2D-Bilanzierung der Fernschubdeformation im östlichen Faltenjura*. Nagra Project Report, NAB 14-105, Nagra, Wettingen.
- Jordan, P., & Nüesch, R. (1989). Deformation structures in the Muschelkalk anhydrites of the Schafisheim Well (Jura Overthrust, northern Switzerland). *Eclogae Geologicae Helvetiae*, 82, 429–454.
- Kälin, D. (1997). Litho- und Biostratigraphie der mittel-bis obermiozänen Bois de Raube-Formation (Nordwestschweiz). *Eclogae Geologicae Helvetiae*, 90, 97–114.
- Kele, S., Breitenbach, S. F. M., Capezzuoli, E., Nele Meckler, A., Ziegler, M., Millan, I. M., et al. (2015). Temperature dependence of oxygen- and clumped isotope fractionation in carbonates: A study of travertines and Tufas in the 6–95°C temperature range. *Geochimica et Cosmochimica Acta*, 168, 172–192. <https://doi.org/10.1016/j.gca.2015.06.032>
- Kim, S. T., & O’Neil, J. R. (1997). Equilibrium and nonequilibrium oxygen isotope effects in synthetic carbonates. *Geochimica et Cosmochimica Acta*, 61, 3461–3475. [https://doi.org/10.1016/S0016-7037\(97\)00169-5](https://doi.org/10.1016/S0016-7037(97)00169-5)
- Kuhlemann, J., & Kempf, O. (2002). Post-Eocene evolution of the North Alpine Foreland Basin and its response to Alpine tectonics. *Sedimentary Geology*, 152, 45–78. [https://doi.org/10.1016/S0037-0738\(01\)00285-8](https://doi.org/10.1016/S0037-0738(01)00285-8)
- Laubscher, H. P. (1978). Foreland folding. *Tectonophysics*, 47, 325–337. [https://doi.org/10.1016/0040-1951\(78\)90037-9](https://doi.org/10.1016/0040-1951(78)90037-9)
- Looser, N., Madritsch, H., Guillong, M., Laurent, O., Wohlwend, S., & Bernasconi, S. (2021). Carbonate clumped isotope and U–Pb data of calcite slickenfibers and veins related to deformation along the basal décollement of the Swiss Jura Mountains, Version 1.0. *Interdisciplinary Earth Data Alliance (IEDA)*. <https://doi.org/10.26022/IEDA/111824>
- Madritsch, H. (2015). Outcrop-scale fracture systems in the Alpine foreland of central northern Switzerland: Kinematics and tectonic context. *Swiss Journal of Geosciences*, 108, 155–181. <https://doi.org/10.1007/s00015-015-0203-2>
- Madritsch, H., Schmid, S. M., & Fabbri, O. (2008). Interactions between thin- and thick-skinned tectonics at the northwestern front of the Jura fold-and-thrust belt (eastern France). *Tectonics*, 27, TC5005. <https://doi.org/10.1029/2008TC002282>
- Malz, A., Madritsch, H., Meier, B., & Kley, J. (2016). An unusual triangle zone in the external northern Alpine foreland (Switzerland): Structural inheritance, kinematics and implications for the development of the adjacent Jura fold-and-thrust belt. *Tectonophysics*, 670, 127–143. <https://doi.org/10.1016/j.tecto.2015.12.025>
- Mangenot, X., Gasparrini, M., Gerdes, A., Bonifacie, M., & Rouchon, V. (2018). An emerging thermochronometer for carbonate-bearing rocks: $\Delta_{47}/(U-Pb)$. *Geology*, 46, 1067–1070. <https://doi.org/10.1130/G45196.1>
- Matter, A., Peters, T., Bläsi, H.-R., Schenker, F., & Weiss, H.-P. (1988a). *Sondierbohrung Schafisheim—Geologie Beilagenband*. Nagra Technischer Bericht 86-03. Landeshydrologie und -geologie, Bern.
- Matter, A., Peters, T., Bläsi, H.-R., Schenker, F., & Weiss, H.-P. (1988b). *Sondierbohrung Schafisheim—Geologie Textband*. Nagra Technischer Bericht 86-03. Landeshydrologie und -geologie, Bern.
- Mazurek, M., Hurford, A. J., & Leu, W. (2006). Unravelling the multi-stage burial history of the Swiss Molasse Basin: Integration of apatite fission track, vitrinite reflectance and biomarker isomerisation analysis. *Basin Research*, 18, 27–50. <https://doi.org/10.1111/j.1365-2117.2006.00286>
- Meckler, A. N., Ziegler, M., Millán, M. I., Breitenbach, S. F. M., & Bernasconi, S. M. (2014). Long-term performance of the Kiel carbonate device with a new correction scheme for clumped isotope measurements. *Rapid Communications in Mass Spectrometry*, 28, 1705–1715. <https://doi.org/10.1002/rcm.6949>

- Müller, I. A., Fernandez, A., Radke, J., van Dijk, J., Bowen, D., Schwieters, J., & Bernasconi, S. M. (2017). Carbonate clumped isotope analyses with the long-integration dual-inlet (LIDI) workflow: Scratching at the lower sample weight boundaries. *Rapid Communications in Mass Spectrometry*, *31*, 1057–1066. <https://doi.org/10.1002/rcm.7878>
- Nemcok, M., Schamel, S., & Gayer, R. (2009). *Thrustbelts: Structural architecture, thermal regimes and petroleum systems* (pp. 1–541). Cambridge University Press. <https://doi.org/10.1017/CBO9780511584244>
- Nuriel, P., Weinberger, R., Kylander-Clark, A. R. C., Hacker, B. R., & Craddock, J. P. (2017). The onset of the dead sea transform based on calcite age-strain analyses. *Geology*, *45*, 587–590. <https://doi.org/10.1130/G38903.1>
- Nuriel, P., Wotzlaw, J.-F., Ovtcharova, M., Vaks, A., Stremtan, C., Sala, M., et al. (2020). The use of ASH-15 flowstone as a matrix-matched reference material for laser-ablation U-Pb geochronology of calcite. *Geochronology*, *3*, 35–47. <https://doi.org/10.5194/gchron-2020-22>
- Ortner, H., Aichholzer, S., Zerlauth, M., Pilser, R., & Fügenschuh, B. (2015). Geometry, amount, and sequence of thrusting in the Subalpine Molasse of western Austria and southern Germany, European Alps. *Tectonics*, *34*, 1–30. <https://doi.org/10.1002/2014TC003550>
- Parrish, R. R., Parrish, C. M., & Lasalle, S. (2018). Vein calcite dating reveals Pyrenean orogen as cause of Paleogene deformation in southern England. *Journal of the Geological Society*, *175*, 425–442. <https://doi.org/10.1144/jgs2017-107>
- Pfiffner, O. A. (1986). Evolution of the north Alpine foreland basin in the Central Alps (Switzerland). In P. A. Allen, & P. Homewood (Eds.), *Foreland basins* (pp. 219–228). Oxford: Blackwell Publishing Ltd. <https://doi.org/10.1002/9781444303810.ch11>
- Pfiffner, O. A. (2014). *Geology of the Alps*. Hoboken, NJ: John Wiley & Sons.
- Pfiffner, O. A. (2017). Thick-skinned and thin-skinned tectonics: A global perspective. *Geosciences (Switzerland)*, *7*(3), 71. <https://doi.org/10.3390/geosciences7030071>
- Philippe, Y., Colletta, B., Deville, E., & Mascle, A. (1996). The Jura fold-and-thrust belt: A kinematic model based on map-balancing. In P. Ziegler, & F. Horvath (Eds.), *Peri-tethys Memoir 2: Structure and prospects of Alpine basins and forelands* (Vol. 170, pp. 235–261). Museum National d'Histoire Naturelle.
- Poblet, J., & Lisle, R. J. (2011). Kinematic evolution and structural styles of fold-and-thrust belts (Vol. 349, pp. 1–24). Geological Society Special Publication. <https://doi.org/10.1144/SP349.1>
- Rittner, M. (2013). *U-Pb dating of brittle deformation* (Unpublished Doctoral Thesis, p. 270). Royal Holloway University of London. [https://pure.royalholloway.ac.uk/portal/en/publications/upb-dating-of-brittle-deformation\(aff86bf1-7949-4184-88c1-886cc509dcf2\).html](https://pure.royalholloway.ac.uk/portal/en/publications/upb-dating-of-brittle-deformation(aff86bf1-7949-4184-88c1-886cc509dcf2).html)
- Roberts, N. M. W., Rasbury, E. T., Parrish, R. R., Smith, C. J., Horstwood, M. S. A., & Condon, D. J. (2017). A calcite reference material for LA-ICP-MS U-Pb geochronology. *Geochemistry, Geophysics, Geosystems*, *18*, 2807–2814. <https://doi.org/10.1002/2016GC006784>
- Schegg, R., Leu, W., Cornford, C., & Allen, P. A. (1997). New coalification profiles in the Molasse Basin of Western Switzerland: Implications for the thermal and geodynamic evolution of the Alpine Foreland. *Ecolgae Geologicae Helvetiae*, *90*, 79–96.
- Schlunegger, F., & Mosar, J. (2011). The last erosional stage of the Molasse Basin and the Alps. *International Journal of Earth Sciences*, *100*, 1147–1162. <https://doi.org/10.1007/s00531-010-0607-1>
- Smeraglia, L., Bernasconi, S. M., Berra, F., Billi, A., Boschi, C., Caracausi, A., et al. (2018). Crustal-scale fluid circulation and co-seismic shallow comb-veining along the longest normal fault of the central Apennines, Italy. *Earth and Planetary Science Letters*, *498*, 152–168. <https://doi.org/10.1016/j.epsl.2018.06.013>
- Smeraglia, L., Fabbri, O., Choulet, F., Buatier, M., Boulvais, P., Bernasconi, S. M., & Castorina, F. (2020). Syntectonic fluid flow and deformation mechanisms within the frontal thrust of a foreland fold-and-thrust belt: Example from the Internal Jura. *Eastern France: Tectonophysics*, *778*, 228178. <https://doi.org/10.1016/j.tecto.2019.228178>
- Sommaruga, A., Burkhard, M., Laubscher, H., Noack, T., & Diebold, P. (1995). Jura Mountains. In *Deep structure of the Swiss Alps* (pp. 45–63). Basel: Birkhäuser. https://doi.org/10.1007/978-3-0348-9098-4_7
- Sommaruga, A., Mosar, J., Schori, M., & Gruber, M. (2017). The Role of the Triassic evaporites underneath the north Alpine foreland. In J. I. Soto, J. F. Flinch, & G. Tari (Eds.), *Permo-Triassic Salt Provinces of Europe, North Africa and the Atlantic Margins* (pp. 447–466). Elsevier Inc. <https://doi.org/10.1016/b978-0-12-809417-4.00021-5>
- Ustaszewski, K., & Schmid, S. M. (2007). Latest Pliocene to recent thick-skinned tectonics at the Upper Rhine Graben—Jura Mountains junction. *Swiss Journal of Geosciences*, *100*, 293–312. <https://doi.org/10.1007/s00015-007-1226-0>
- Vermeesch, P. (2018). IsoplotR: A free and open toolbox for geochronology. *Geoscience Frontiers*, *9*, 1479–1493. <https://doi.org/10.1016/j.gsf.2018.04.001>
- Von Hagke, C., Cederbom, C. E., Oncken, O., Steckli, D. F., Rahn, M. K., & Schlunegger, F. (2012). Linking the northern Alps with their foreland: The latest exhumation history resolved by low-temperature thermochronology. *Tectonics*, *31*, TC5010. <https://doi.org/10.1029/2011TC003078>
- Willett, S. D., & Schlunegger, F. (2010). The last phase of deposition in the Swiss Molasse Basin: From foredeep to negative-alpha basin. *Basin Research*, *22*, 623–639. <https://doi.org/10.1111/j.1365-2117.2009.00435>
- Ziegler, P. A., & Fraefel, M. (2009). Response of drainage systems to Neogene evolution of the Jura fold-thrust belt and Upper Rhine Graben. *Swiss Journal of Geosciences*, *102*, 57–75. <https://doi.org/10.1007/s00015-009-1306-4>